Motion of rotating pairs in a hexagonal superlattice pattern within dielectric barrier discharge

Lifang Dong, Ben Li, Zhongkai Shen, Yongjie Wang, and Ning Lu

Phys. Rev. E **86**, 036211 — Published 20 September 2012

DOI: 10.1103/PhysRevE.86.036211

Motion of rotating pairs in a hexagonal superlattice pattern within dielectric barrier discharge

Lifang Dong, Ben Li, Zhongkai Shen, Yongjie Wang, and Ning Lu

College of Physics Science and Technology, Hebei University, Baoding 071002, China and Hebei Key Laboratory of Optic-electronic Information Materials, Baoding 071002, China

Stochastic rotation of rotating pairs in a hexagonal superlattice pattern is observed in a dielectric barrier discharge system. It is found that the pairs rotate with orientation and diameter randomly changing by observing a series of frames recorded by a high speed video camera. Frames recorded by a high speed framing camera with exposure time corresponding to current pulse phases in one half cycle of the applied voltage show that one rotating spot, six small spots and another rotating spot in one cell discharge successively. Based on this discharging sequence, forces exerted on a rotating spot are analyzed at different discharging stages in a half voltage cycle. A resultant force on a rotating spot with both magnitude and direction varied leads to the stochastic rotation.

PACS numbers: 52.80.Tn, 47.54.-r, 89.75.Kd

As a nonlinear self-organized phenomenon, pattern formation not only exists abundantly in nature but also has been researched in many experimental systems such as Faraday systems, reaction-diffusion systems, nonlinear optical systems and dielectric barrier discharge (DBD) systems [1-17]. In recent years, patterns in dielectric barrier discharge are gaining widespread attention [7-17]. Generally, AC voltage frequency for pattern formation in DBD ranges from 10 kHz to 200 kHz, corresponding to the cycle range from 5 μs to 100 μs. Accordingly, the investigation can be conducted on microscopic scales that approximate to one or several voltage cycles and macroscopic ones that naked eyes can follow. Many static and dynamic patterns have been studied in different aspects which are mainly concerned with the whole patterns on either microscopic or macroscopic scales. Purwins et al observed

the transition of a rigid-body rotating hexagonal pattern and proved its dynamics to be thermosensitive [12]. Breazeal et al investigated many controlled parameters such as vapor level and drive frequency for static and dynamic patterns emerging [13]. Boeuf et al analyzed the time evolution of a honeycomb pattern through images taken by an ICCD camera in a half voltage cycle [14]. We studied a colliding-pairs hexagonal superlattice pattern (CPHSP) with dynamic spots nesting in a hexagonal framework constituted by stationary spots both microscopically and macroscopically [15]. In this work, we will present microscopic motion behaviors of dynamic spots in the rotating-pairs hexagonal superlattice pattern (RPHSP), whose macroscopic behaviors have been studied previously [16,17].

Both the motion of dynamic spots and the stability of static spots should be determined by interactions between discharging spots [18-21]. Purwins et al investigated the motion of traveling pairs of spots by developing a detailed comprehension of the coupling of neighboring ignition processes [20]. Shirafuji et al studied Coulomb force and Lorentz force between a few localized filaments discharging synchronously [21]. In this work, we devote to analyze forces exerted on an unbalanced spot by other spots to interpret its motion.

For analyzing filament interactions, the discharging sequence [14,22,23] of a pattern should be emphasized, which can decide the synchronous ignited spots and the precedence of asynchronous ignited spots. Furthermore, it is necessary to distinguish forces between surface charges from those between space filaments for interaction analysis.

In this paper, we report on the stochastic rotation of rotating pairs in RPHSP. Diameter and rotation angular velocity of pairs are investigated. By using a high speed framing camera, the discharging sequence of the pattern is shown, based on which the forces exerted on one rotating spot are analyzed to interpret its motion. Generally, this work explores the frontier for interactions on unbalanced plasma filaments and their motion behaviors in complex superlattice patterns.

The schematic diagram of the experimental setup is shown in Fig. 1. The following is a brief description. Two cylindrical containers with diameter of 75 mm

and sealed with 1.5 mm thick glass plates are filled with water. A metallic ring immerses in each of the containers and is connected to an AC power supply with 53 kHz driven frequency, corresponding to 18.9 μs driven cycle. Thus, the water acts as liquid electrode and the glass plates serve as dielectric layers. A circular glass frame with 1.6 mm thickness is placed between the two parallel glass plates. All of the apparatus are enclosed in a big container filled with air/argon mixture. The gas pressure is varied from 76 Torr to 760 Torr. The amplitude of driven voltage can be measured by a high-voltage probe (Tektronix P6015A 1000X) and recorded by an oscilloscope (Tektronix TDS3054B). An ordinary camera is used to take photographs of discharging patterns with long exposure. A high speed video camera (HSVC pco. dimax 9000000207) is used for statistics of motion behaviors of rotating pairs for it can keep records as long as needed. Frames with exposure less than 40 μs are not clear enough for detailed analysis due to limited sensitivity of the camera and weak light intensity of filaments. Statistical results presented in this paper are based on frames with 40 μs exposure and 8 μs delay. A high speed framing camera (HSFC pro. 120PH0047) is used to study the discharging sequence. It has three photographing channels and can record three successive frames corresponding to current pulse phases of 100 ns orders.

The hexagonal superlattice structure discussed in this paper has one big spot (hollow ring) nesting in each hexagonal cell of the framework constituted by small fixed spots, as shown in Fig. 2. It is named as rotating-pairs hexagonal superlattice pattern because one big spot is actually composed of a pair of rotating spots which can be seen on short time scales. Fig. 3 presents a series of enlarged frames of RPHSP recorded by HSVC with 40 μs exposure and 8 μs delay. The pair denoted by "○" rotates clockwise and anticlockwise with varied speed. It generally rotates slightly [Figs. 3(a-c) and 3(d-f)] but occasionally with a large angular displacement [Figs. 3(c-d)]. Meanwhile, the diameter (distance between two spots in one pair) changes temporally as well, which can be distinguished by different sizes of the circles denoting the pair. Depending on these phenomena, the motion of the pair should be described as rotation with stochastic variation of diameter and angular velocity. In the

following, statistics of distance D and rotation angular velocity $\boldsymbol{\omega}$ are mainly investigated.

Fig. 4(a) shows the distance D between two spots in one rotating pair as a function of time t. It can be seen clearly that the distance fluctuates with time in an approximate range from 0.7 mm to 1.4 mm. And this result demonstrates our previous prediction that pairs should rotate with radius varying due to a varied radial force exerted on one rotating spot [17]. The probability distribution function (PDF) of D in Fig. 4(b) turns out that the peak is in the range from 0.8 mm to 1.0 mm. Through abundant statistics, the most probable value may actually vary from 0.8 mm to 1.2 mm.

Fig. 5(a) shows the angular difference θ between instantaneous orientations of one pair in two neighboring frames as a function of time t. It is found that θ value changes randomly with time in an approximate range -1.5 rad~1.5 rad, in which negative and positive signs represent clockwise and anticlockwise rotation directions respectively, and that many small angular differences and a few large ones take place by turn. The angular velocity $\boldsymbol{\omega}$ is calculated by θ values in Fig. 5(a) divided by time interval and its PDF is shown in Fig. 5(b). It is obvious that the peak is in the range from -500 rad/s to 500 rad/s. For showing the peak in detail and comparing with our previous work [17], the PDF of $\boldsymbol{\omega}$ in the range -600rad/s~600rad/s approximately corresponding to angle difference -10°~10° is shown in Fig. 5(c). The result is quite different from that calculated by the length of camber trajectories divided by ms-scale exposure time, which is based on the supposition that pairs only rotate in one direction. However, they actually rotate with direction randomly changing, leading to overlying of repeated rotation which makes no contribution to the length of the observable trajectory.

In the following, forces exerted on one rotating spot will be analyzed to interpret the mechanism of the varied velocity rotation. Due to the asynchrony of filamentary discharges in patterns, forces should be analyzed in different discharging stages determined by the discharging sequence. Actually, the discharging sequence of RPHSP has been obtained by measurements of correlations between discharge

filaments using photoelectric multiplier tubes [16]. There are three discharging current pulses in each half voltage cycle, corresponding to the discharging sequence that one rotating spot discharges first, then the static small spots, finally another rotating spot. For displaying the sequence more intuitively, it is investigated by HSFC here.

Figs. 6(a)-6(c) show the frames of RPHSP recorded by HSFC with exposure time corresponding to the three current pulse phases in each half voltage cycle respectively and integrated over 20 voltage cycles to get enough light signals. The three channels of HSFC actually have different sensitivities. The channel with low sensitivity is used for recording the sublattice of small spots because the light intensity of static small spots can integrate over many cycles in relatively fixed positions and therefore are higher than that of rotating spots. Comparing Figs. 6(a) and 6(c) with Fig. 6(b), it is obvious that static small spots and rotating spots are of different sublattices. Rotating spots in Fig. 6(a) are bigger than static spots and some of spots in Figs. 6(c) seem diffused. In fact, during the bifurcation process from hexagonal pattern to hexagonal superlattice pattern, some spots interact pairwise and become rotating pairs while the rest become static spots constituting the hexagonal framework. All of them discharge once in each half voltage cycle and they are nearly the same size. Therefore rotating spots have no intrinsic difference with static ones in the superlattice. Bigger sizes and diffusion of rotating spots should be both attributed to their movements. Further, the diffusion of some spots in Fig. 6(c) indicates that large position changes of these spots mainly occur during the third pulse phase in a half voltage cycle. Fig. 6(d) gives the superposition of Figs. 6(a) and 6(c). Position differences of the paired spots illustrate that they are of different discharging sublattices. Moreover, some overlapped parts between paired spots result from the superposition of spots ignited in different half voltage cycles.

As is well known, discharging spots in patterns include wall charge stacks on dielectric surfaces [24] and space plasma filaments [25]. Coulomb force exists between charges and Lorentz force exists between synchronous plasma filaments. In time intervals between ignitions, there are only Coulomb forces between wall charge stacks of spots. Forces between unburned spots and between burned spots are both

repulsive while those between unburned and burned ones are attractive. During breakdown phases, Lorentz forces exist between current filaments of burning spots and Coulomb forces exist between all charges (wall charges and space charges in filaments). Lorentz forces are always attractive because of the same direction of burning currents. Coulomb forces between burning and unburned spots are repulsive at first with magnitudes decreasing to zero and then attractive with magnitudes increasing to certain values due to the gradually inverted wall charge fields. And Coulomb forces between burning and burned ones are just in the opposite way.

Considering that both Lorentz force and Coulomb force decrease fast with the interaction distance increasing, forces exerted on one rotating spot by other nearby spots in the same cell are considered at first for simplicity. Coulomb forces between wall charge stacks are available for all the time and those between space charges and wall charge stacks during breakdown phases should be considered as well. There is no Lorentz force on a rotating spot for it discharges asynchronously with all the other spots in the same cell according to the sequence.

Fig.7 shows the schematic diagrams of the force analysis on one rotating spot of one pair with a random instantaneous orientation (not along the symmetry axes) in three time intervals in one half cycle of the applied voltage: only one rotating spot discharged [Fig.7 (a)], one rotating spot and all small spots discharged [Fig.7 (b)], and the whole cell discharged [Fig.7 (c)], respectively. In each diagram, all the spots are of positive charges (labeled as "●") before discharging but negative (labeled as "○") after that. $\mathbf{F}_0$ and $\mathbf{F}_1$-$\mathbf{F}_6$ are the forces exerted by anther rotating spot and the six small spots, respectively. If Coulomb force equation for point charges is used for calculation, forces decay fast enough with distance increasing so that those exerted by nearer spots are schematically drawn much longer than those exerted by farther spots in the diagrams. In fact, wall charges in patterns have a certain kind of distribution and the distance between spots is not long enough, so wall charge stacks may not be considered as point charges. But it is believed that forces should be inversely proportional to no less than 2 powers of distance and therefore the magnitudes of these forces may have larger differences.

Obviously, only tangential force components with direction changing can prompt the spot changing its rotation direction, so tangential projections of related forces should be investigated. $\mathbf{F}_0$ has no tangential projection due to its permanent radial direction and $\mathbf{F}_r$ is the resultant force of $\mathbf{F}_1$-$\mathbf{F}_6$, whose tangential component is $\mathbf{F}_{r,\perp}$. The change of direction of $\mathbf{F}_{r,\perp}$ is obvious by comparing the three diagrams. And it is not difficult to imagine that the magnitude will also change when the pair changes its orientation. During breakdown phases, the burning process of spots associated with space charges transporting and the corresponding wall charge fields inverting gradually will make $\mathbf{F}_{r,\perp}$ varied as well. In a word, $\mathbf{F}_{r,\perp}$ changes temporally in both of direction and magnitude, leading to the varied velocity rotation.

Furthermore, referring to the analysis that the rotation of one pair can induce rotation of nearby pairs during the bifurcation process [17], forces exerted by nearby pairs should be considered as well. However, force analysis shows that these additional forces do not change the above result that $\mathbf{F}_{r,\perp}$ changes with time because they have much smaller magnitudes than those in Fig. 7. Besides, twenty-four forces including Coulomb forces and Lorentz forces should be added to each force diagram in this consideration because each pair has six nearby pairs. This addition makes the diagrams very chaotic, so force diagrams with these forces are not presented here for simplicity.

In conclusion, stochastic rotation of rotating pairs in RPHSP is studied in this paper. Diameter D is fluctuant temporally due to varied radial forces and abundant statistics shows that the most probable value varies from 0.8 mm to 1.2 mm. Angular difference θ as a function of t indicates rotation with velocity stochastically changing. The velocity range calculated on 50 μs scale is quite different from that calculated by the length of trajectories divided by ms-scale exposure time due to that overlying of repeated rotation makes no contribution to trajectory lengths. Frames of discharging sequence are recorded by HSFC and are compared with each other. Diffusion of rotating spots is attributed to their movement. Based on the sequence, force analysis in one half voltage cycle is conducted and indicates that a tangential component of forces exerted on rotating spots changes temporally, leading to the varied velocity

rotation.

It is very important to note that we can just try to understand the motion observed from frames with 40 μs exposure by force analysis in one half voltage cycle of μs scale at present due to the limited sensitivity of HSVC. In the next work, we will develop the μs-scale investigation of the motion behavior of rotating pairs for more details. All in all, the rotating-pairs hexagonal superlattice pattern is so complex a discharging structure that the motion of the pairs and the varied forces are influenced by abundant spatiotemporal factors such as discharging sequence, wall charge quantities and their distribution, orientations and diameters of pairs, inverted wall charge fields during breakdown phases. This paper is just the tip of the iceberg and in the future we will do our best to develop a whole set of knowledge hierarchy of interactions on unbalanced discharging spots and their motion behaviors in static-dynamic interleaving superlattice patterns including RPHSP.

This work is supported by the National Natural Science Foundation of China under Grant Nos. 11175054 and 10975043, the Natural Science Foundation of Hebei Province, China, under Grant No. A2010000185, the Research Foundation of Education Bureau of Hebei Province, China, under Grant No. ZD2010140, Key basic research project in application basic research plan of Hebei Province under Grant No.11967135D, and the Specialized Research Fund for the Doctoral Program of Higher Education, State Education Ministry of China (No. 20101301110001).

[1] A. von Kameke, F. Huhn, G. Fernández-García, A. P. Muñuzuri, and V. Pérez-Muñuzuri, Phys. Rev. E **81**, 066211 (2010).

[2] G. Fernández-García, D. I. Roncaglia, V. Pérez-Villar, A. P. Muñuzuri, and V. Pérez-Muñuzuri, Phys. Rev. E **77**, 026204 (2008).

[3]A. Rabinovitch, Y. Biton, D. Braunstein, M. Friedman, and I. Aviram, Phys. Rev. E **85**, 036217 (2012).

[4] Anne J. Catllá, Amelia McNamara, and Chad M. Topaz, Phys. Rev. E **85**, 026215 (2012).

[5] Cheng Hou Tsang, Boris A. Malomed, and Kwok Wing Chow, Phys. Rev. E **84**,

066609 (2011).

[6] Nir Dror, Boris A. Malomed, and Jianhua Zeng, Phys. Rev. E **84**, 046602 (2011).

[7] Lifang Dong, Weili Fan, Yafeng He, Fucheng Liu, Shufeng Li, Ruiling Gao, and Long Wang, Phys. Rev. E **73** 066206 (2006).

[8] Xiaoxi Duan, Jiting Ouyang, Xiaofei Zhao, and Feng He, Phys. Rev. E **80**, 016202 (2009).

[9] J. Sinclair and M. Walhout, Phys. Rev. Lett. **108**, 035005 (2012).

[10] Xiaoxi Duan, Shaowei Xu, Jian Liu, Feng He, and Jiting Ouyang, IEEE Trans. Plasma Sci. **39**(11), 2074-2075 (2011).

[11] Yan Feng, Chunsheng Ren, Qiuyue Nie, and Dezhen Wang, IEEE Trans. Plasma Sci. **38**(5), 1061-1065 (2010).

[12] A. L. Zanin, E. L. Gurevich, A. S. Moskalenko, H. U. Bödeker, and H.-G. Purwins, Phys. Rev. E **70**, 036202 (2004).

[13] W. Breazeal, K. M. Flynn, and E. G. Gwinn, Phys. Rev. E **52**(2), 1503-1515 (1995).

[14] B. Bernecker, T. Callegari, S. Blanco, R. Fournier, and J.P. Boeuf, Eur. Phys. J. Appl. Phys. **47**, 22808 (2009).

[15] Lifang Dong, Ben Li, Ning Lu, Xinchun Li, and Zhongkai Shen, Phys. Plasmas, **19**, 052304 (2012).

[16] Lifang Dong, Ruiling Gao, Yafeng He, Weili Fan, and Weili Liu, Phys. Rev. E **74**, 057202 (2006).

[17] Lifang Dong, Yujie Yang, Ben Li, Weili Fan, and Qian Song, Phys. Plasmas **18**, 122101 (2011).

[18] L. Stollenwerk, New J. Phys. **11**, 103034 (2009).

[19] L. Stollenwerk, Plasma Phys. Control. Fusion **52**, 124017 (2010).

[20] I. Brauer, M. Bode, E. Ammelt, and H.-G. Purwins, Phys. Rev. Lett. **84**(18), 4104-4107 (2000).

[21] Tatsuru Shirafuji, Takayuki Kitagawa, Tatsuro Wakai, and Kunihide Tachibana, Appl. Phys. Lett. **83**(12), 2309 (2003).

[22] J. Guikema, N. Miller, J. Niehof, M. Klein, and M. Walhout, Phys. Rev. Lett.

85(18), 3817-3820 (2000).

[23] M. Klein, N. Miller, and M. Walhout, Phys. Rev. E **64**, 026402 (2001).

[24] L. Stollenwerk, J. G. Laven, and H.-G. Purwins, Phys. Rev. Lett. **98**, 255001 (2007).

[25] N Merbahi, N Sewraj, F Marchal, Y Salamero and P Millet, J. Phys. D: Appl. Phys. **37** 1664–1678 (2004).

Fig.1. Schematic diagram of the experimental setup.

Fig.2. (Color online) A photograph of RPHSP taken by an ordinary camera with exposure time t_E=40 ms. Experimental parameters: discharge gap d=1.6 mm, gas pressure p=380 Torr, fraction of argon φ=60%, applied voltage U=5.8 kV, frequency of applied voltage f=53 kHz, corresponding to the driven cycle of 18.9 μs, power density P_0=2 W/cm^2.

Fig.3 (Color online) A series of enlarged frames of RPHSP. Exposure time t_E=40 μs, delay time t_D=8 μs. The different sizes of the circles denoting the pair indicate the varied rotation diameter.

Fig.4. (Color online) Statistics of distance D between two spots in one rotating pair. (a) D as a function of time t. (b) Probability distribution function (PDF) of D.

Fig.5. (Color online) Statistics of rotation angular difference θ and the corresponding $\boldsymbol{\omega}$ value. (a) θ as a function of time t. Clockwise and anticlockwise rotation directions are represented by negative and positive signs respectively. (b) PDF of $\boldsymbol{\omega}$ calculated by θ in (a) divided by time interval. (c) PDF of $\boldsymbol{\omega}$ in a shorter range -600rad/s~600rad/s approximately corresponding to the angle difference -10°~10°.

Fig.6. (Color online) Discharging sequence of RPHSP. (a) Frame of one set of rotating spots. (b) Frame of small static spots. (c) Frame of another set of rotating spots. These frames are recorded by HSFC with exposure time corresponding to the three current pulse phases in each half voltage cycle respectively and integrated over 20 voltage cycles to get enough light signals. (d) The frame is the superposition of red colored (a) and green colored (c), which illustrates that the two spots in the same pair are of different sublattices.

Fig.7. (Color online) Schematic diagrams of force analysis on the wall charge stack of one rotating spot on the dielectric surface of the positive electrode in three different situations. (a) One rotating spot has discharged. (b) One rotating spot and all small spot have discharged. (c) The whole cell experienced discharge once. In each diagram, positive charge spots are labeled by "●" while negative ones labeled by "○". $\mathbf{F}_0$, $\mathbf{F}_1$-$\mathbf{F}_6$, $\mathbf{F}_r$, and $\mathbf{F}_{r,\perp}$ are the force exerted by anther rotating spot, the forces exerted by small spots, the resultant force of $\mathbf{F}_1$-$\mathbf{F}_6$, and the tangential component of the resultant force, respectively.

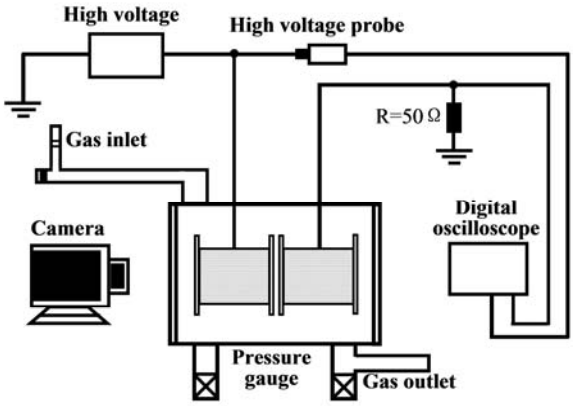
High voltage
High voltage probe
R=50 Ω
Gas inlet
Camera
Digital
oscilloscope
Pressure
gauge
Gas outlet

Fig. 1

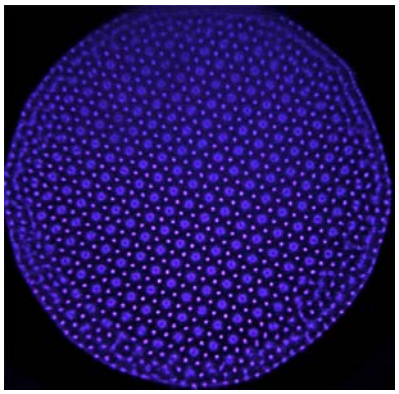

Fig. 2

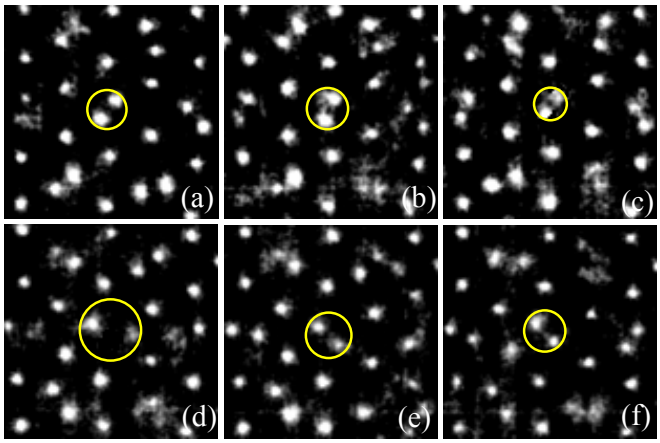

Fig. 3

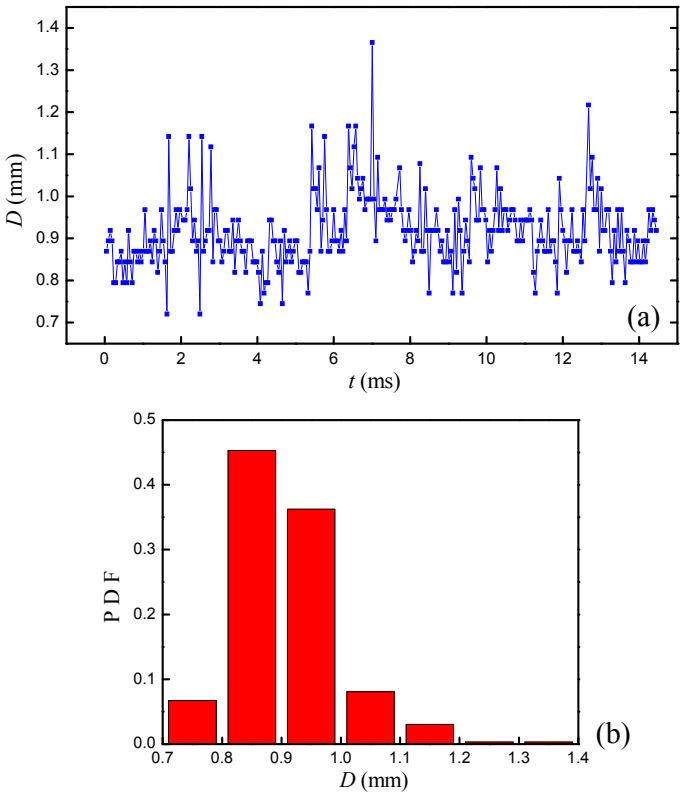

Fig. 4

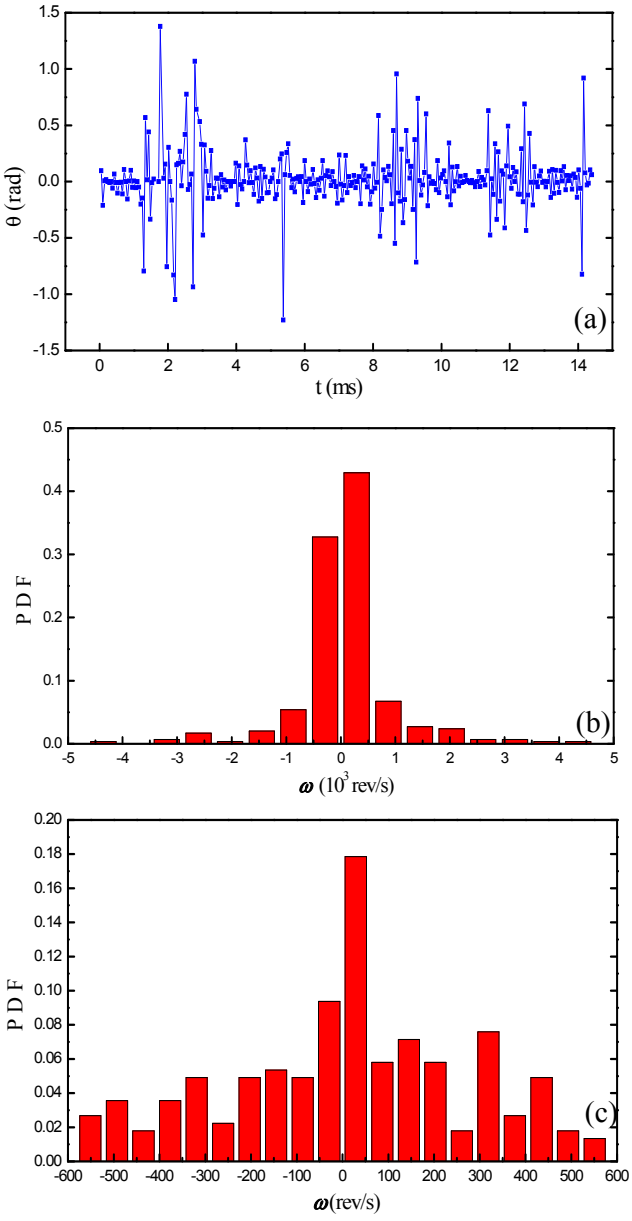

Fig. 5

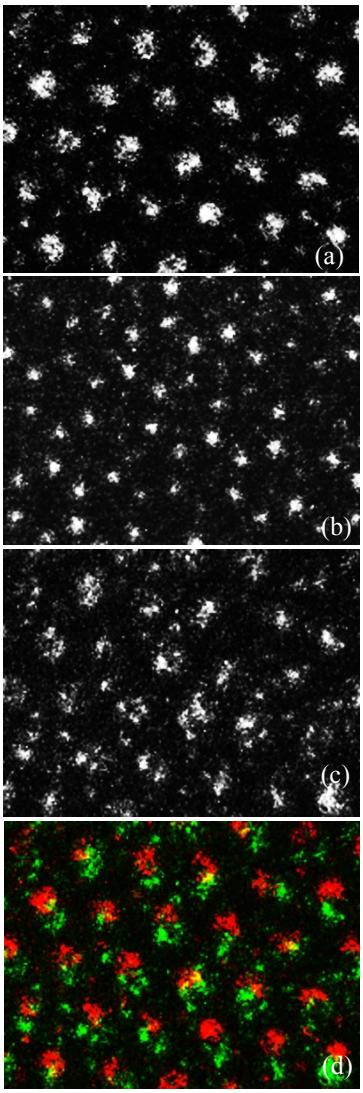

Fig. 6

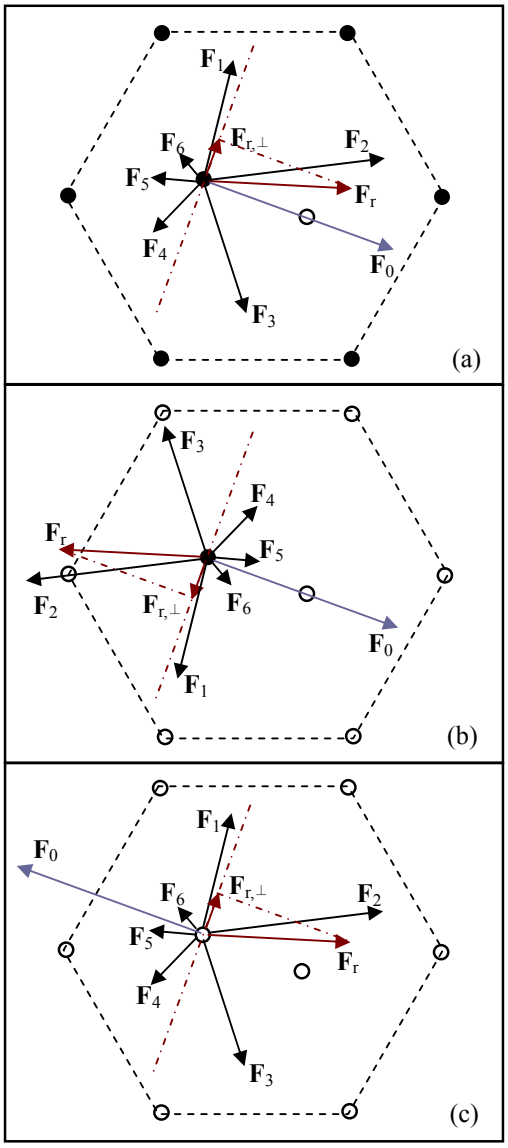
F1
F6
Fr,⊥
F2
F5
Fr
F4
F0
F3
(a)
F3
F4
Fr
F5
F2
Fr,⊥
F6
F0
F1
(b)
F0
F1
F6
Fr,⊥
F2
F5
Fr
F4
F3
(c)

Fig. 7